Journal of Materials Chemistry C

Accepted Manuscript

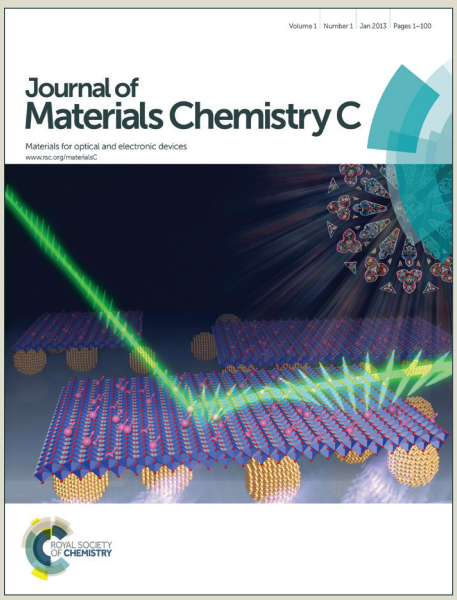

ROYAL SOCIETY OF CHEMISTRY

www.rsc.org/materialsC

Photoluminescence and Raman Mapping Characterization of WS_2 Monolayers Prepared in Top-Down and Bottom-Up Methods

X. H. Wang,[1, 2, 3] J. Q. Ning,[1, 2, 3] C. C. Zheng,[1, 4] B. R. Zhu,[1] L. Xie,[1] H. S. Wu [1] and S. J. Xu[*, 1, 2, 3]

[1]*Department of Physics,* [2]*HKU-Shenzhen Institute of Research and Innovation (HKU-SIRI),* [3]*HKU-CAS Joint Laboratory on New Materials, The University of Hong Kong, Pokfulam Road, Hong Kong, China*

[4]*Mathematics and Physics Centre, Department of Mathematical Sciences, Xi'an Jiaotong-Liverpool University, Suzhou 215123, China*

Two kinds of tungsten disulfide (WS_2) monolayers respectively prepared in top-down and bottom-up approaches are studied with Raman and photoluminescence (PL) mapping techniques. By mapping the intensity of the two characterized phonon modes of WS_2, the monolayer region can be quickly selected, which is more conclusive than by comparing the small shift in phonon peak position. On the other hand, PL mapping yields more information regarding the uniformity and quality of the monolayers than Raman mapping. We also show that the focused laser may cause substantial damage to the crystal lattice of monolayers for long duration mapping.

Key Words: Monolayers, tungsten disulfide, photoluminescence, Raman scattering, mapping

[*]E-mail: sjxu@hku.hk

Introduction

Since the emergence of two-dimensional (2D) materials, experimentally unambiguous identification of atomically thin monolayers has always been vital for further studies and applications of these ultimate 2D materials. Although optical interference is extremely useful in finding thin layers, it is still not conclusive for the determination of monolayers. Various other techniques have been thus developed. Among them, atomic force microscopy (AFM) is a straight forward choice to identify thickness of atomic layers and has been successfully applied since the discovery of graphene.[1] Due to the drawbacks of AFM, however, especially the slow scanning speed and time consuming, Raman spectroscopy has been then developed as a much easier and faster approach in studying the layers of graphene.[2-4] It is worth noticing that accurate structural determination of the atomically thin monolayer thickness with AFM etc. still represents a challenging task due to the resolution limit of these techniques.

For recently developed 2D transition metal dichalcogenides (MX_2), strong photoluminescence (PL) due to the transition from indirect to direct band gap semiconductor is also an important indication for monolayers, which was firstly reported in MoS_2.[5] For WS_2, the strong PL at room temperature has been studied for monolayers obtained via different methods.[6-11] Theoretical and experimental reports [12, 13] proposed that the emission is attributed to exciton recombination as a result of large exciton binding energy and quantum confinement effect. Meanwhile, the layer dependence of Raman spectrum has also been established for MX_2[15-20], which can be classified as the shift or intensity change in the Raman modes of inter-layer and in-plane vibrations.[15-17] Almost every study on 2D MX_2 has presented Raman spectroscopy as a crucial supporting evidence to identify monolayers, but there is an inconsistency between various experimental reports on the Raman shift.[6, 7] And the theoretical work[15] calculating Raman shift based on density functional perturbation theory agrees with experimental study in the overall trend,[16] but still there is an obvious mismatch with the actual data for layer dependence. Moreover, for WS_2, the experimental report[7] for the shift in Raman mode between the bulk material and monolayer is only 0.5 cm^{-1} for E^1_{2g} mode and 3 cm^{-1} for

A_{1g} mode. With great potential in the real application of 2D dichalcogenides[21-24], an in-depth investigation on Raman and PL signals of monolayer MX_2 is highly desirable.

In this article, we report a state-of-the-art investigation of direct and conclusive identification of the monolayer region by Raman mapping on the intensity change of A_{1g} for two kinds of WS_2 monolayers prepared with top-down and bottom-up methods. Meanwhile, we also compare PL and Raman mapping and show that PL mapping gives a better resolution regarding the quality and uniformity of the monolayer.

Experimental

As mentioned above, the two kinds of WS_2 monolayers were prepared with top-down and bottom-up methods, respectively. The first kind were the mechanically exfoliated WS_2 monolayer flakes obtained from a bulk crystal via detaching by an adhesive tape and then transferring onto Si substrate, whereas the second kind were the WS_2 monolayer triangles directly synthesized on Si substrate in a hot-wall furnace by employing high purity WO_3 and sulfite powder as the starting materials. The latter growth method that is a bottom-up technique is similar to the chemical vapor deposition (CVD) growth of MoS_2 reported by Lee et al.[17] The Raman and photoluminescence (PL) spectroscopic and mapping characterization was carried out at room temperature on a WITec scanning confocal microscopy system integrated with an Acton monochromator + an Andor CCD detector. The excitation source was a 514.5 nm argon ion laser which is guided into the system by optical fiber and focused by a 60x Nikon objective.

Results and discussion

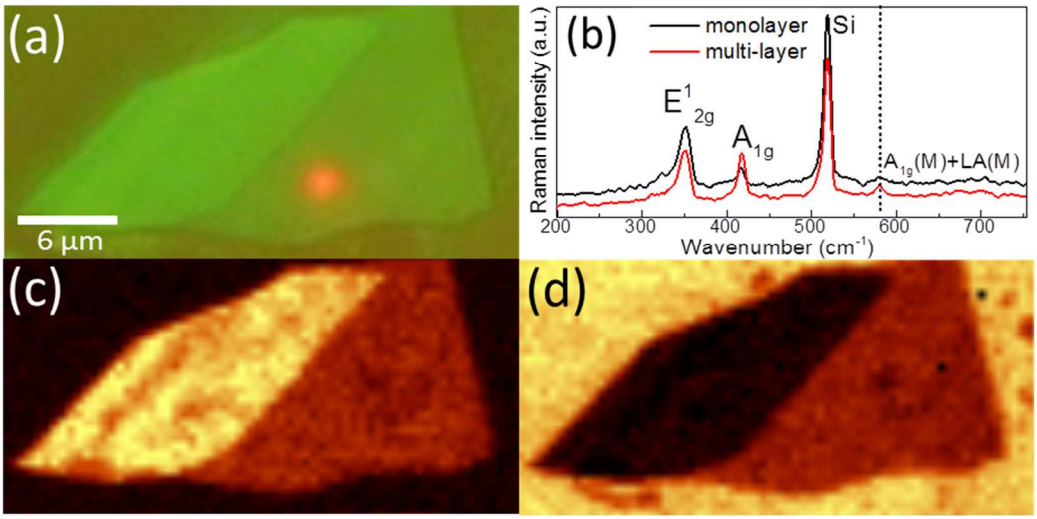

Figure 1 (a) Optical image of the mechanically exfoliated WS_2 flake. The red spot is the photoluminescence image of the single layer under the excitation of 514.5 nm laser; (b) Raman spectra of monolayer and the multi-layer region. (c) Raman mapping with respect to the Raman mode A_{1g} of the WS_2 flake; and (d) the Raman mode (519.6cm^{-1}) of the silicon substrate.

Figure 1(a) shows the optical image of the WS_2 flake mechanically exfoliated from a bulk crystal of tungsten disulfide. Clearly, the flake consists of two regions: The right side in the optical image is the monolayer region where the red spot is the strong light emission excited by the 514.5 nm argon laser which has been blocked by the notch filter, whereas the left side is a few-layer region. Figure 2(b) depicts the Raman spectra of the two characteristic phonon modes of WS_2 taken from the two different regions. For the in-plane vibration mode E^1_{2g}, the peak positions were located at 351.1 cm^{-1} and 350.7 cm^{-1} for the monolayer and few-layer regions, respectively. It is interesting to notice that a n unusual resonant excitation of the second-order longitudinal acoustic phonon (2LA(M)) in WS_2 monolayer was claimed to be observed by Berkdemir *et al.*'s using the 514.5nm excitation line.[16] This second-order Raman peak happens to be very close to the E^1_{1g} peak. In our Raman spectral data as shown in Figure 2(b), the E^1_{1g} peak shows an asymmetric

lineshape with a lower wavenumber tail. One composite transition of this acoustic LA(M) with an optical phonon Raman peak is observed at around 582 cm^{-1} (marked in a vertical dashed line) in Figure 1(b) for our monolayer WS_2. On the other hand, the inter-layer (out of plane) vibration mode A_{1g} peak shifted from 418.2 cm^{-1} to 417.1 cm^{-1} for moving the laser excitation spot from the few-layer region to the monolayer region, which is consistent with other experimental observation[15] and theoretical calculations.[14] The most noticeable difference in the Raman spectra is the intensity change between the two phonon modes. We recorded a peak intensity ratio around 3.5 which is in good agreement with Berkdemir *et al*.'s on the identification of WS_2 monolayer.[16] In fact, the monolayer region of the WS_2 flake can be directly determined by the means of Raman mapping. Figure 1(c) shows the Raman mapping with respect to the A_{1g} mode. In the Raman image, the monolayer region has a sharp contrast compared with the multi-layer region where the intensity of A_{1g} mode. As a reference, mapping the Raman scattering intensity of the silicon phonon mode can also enable us determine the WS_2 monolayer region, such as the dark red region as shown in Figure 1(d).

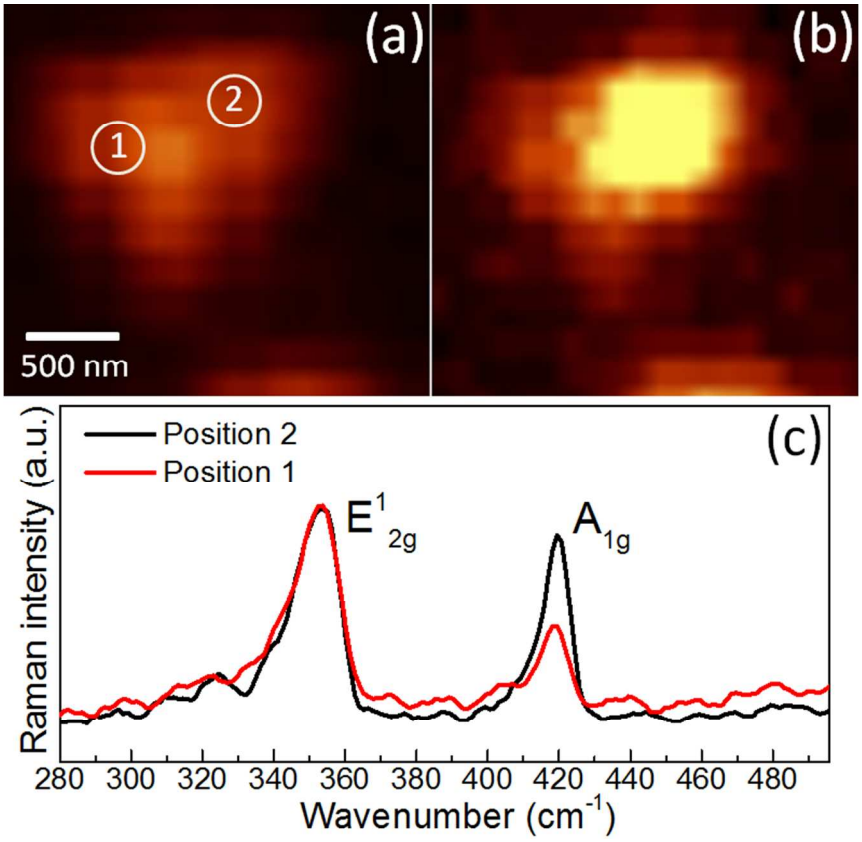

Figure 2. Raman mapping of the E^1_{2g} mode (a) and A_{1g} mode (b) for a WS_2 triangle prepared with bottom-up method. Raman spectra (c) taken at two positions marked in Fig. 2(a).

For a comparative study purpose, we have also conducted micro-Raman mapping on WS_2 triangles directly grown on Si with bottom-up method. We selected a WS_2 triangle with multilayer on one corner (i.e., the upper right corner in Figure 2(b)) and the rest region of monolayer for conducting Raman mapping measurement. Figure 2(a) and 2(b) show the Raman mapping for the characteristic Raman modes of E^1_{2g} and A_{1g}, respectively. From the two images, we can immediately see the bright A_{1g} Raman signal in the multilayer region which is in agreement with the case of WS_2 flake prepared with top-down method. The Raman spectra measured at two different positions, i.e., position (1) and (2) in Figure 2(a), were depicted in Figure 2(c). Again, the Raman spectra show noticeable difference in intensity between the two characteristic modes for monolayer and multilayer. For the

peak position, E^1_{2g} mode is the almost identical for both the positions, whereas there is 1.2 cm^{-1} redshift for A_{1g} mode from the position (2) (multilayer) to the position (1) (monolayer). So far, we have clearly demonstrated that for both kinds of WS_2 samples prepared in top-down and bottom up approaches, intensity change between the two characteristic modes is more conclusive than the peak position change in the Raman identification of monolayer. Moreover, mapping the Raman scattering intensity of the inter-layer mode A_{1g} offers a much easier and straight-forward method to find the monolayer region.

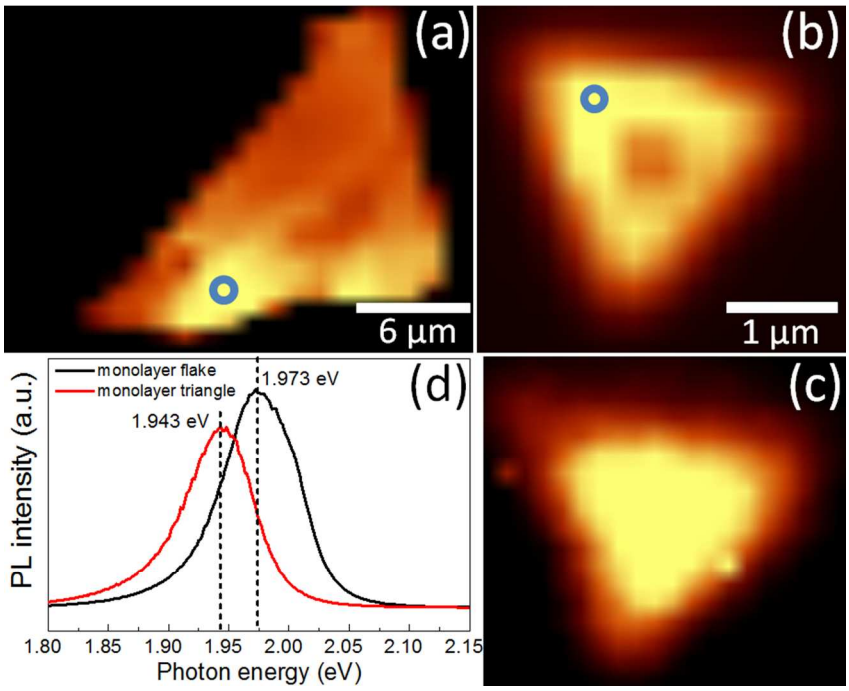

Figure 3. PL mapping images: The monolayer flake (a) and a monolayer triangle (b); The same triangle is mapped with respect to the A_{1g} Raman mode (c); PL spectra measured at the brightest regions indicated by the blue circles in (a) and (b) for both the samples (d).

As mentioned in the introduction part, intense light emission is another optical signature of MX_2 monolayers due to the nature of direct bandgap, and thus can be employed as another identifying tool for monolayers. The PL mapping image of the mechanically exfoliated WS_2 flake is shown in Figure 3(a). Comparing with the Raman mapping of the

same sample shown in Fig. 1(c) and 1(d), PL mapping obviously yields more information regarding the uniformity of the monolayer region. The variation of PL intensity in the monolayer region of the flake can be as large as 15% with respect to the highest intensity, whereas the variation in the triangle sample is even more noticeable as shown in Figure 3(b). As a result of large exciton binding energy[12, 13], the PL emission at room temperature should be still of excitonic nature. However, the broad PL band may consist of both free exciton emission and defect bound exciton emission. Meanwhile, some defects may act as "PL kill centers" that offer various non-radiative channels causing the overall PL intensity drop. Hence the uneven distribution of defects may result in the non-uniformity in PL intensity mapping. It is also of interest for us to make a comparison between PL mapping and Raman mapping for a monolayer triangle prepared in bottom-up approach. Figure 3(c) shows the Raman mapping image of the inter-layer vibration mode A_{1g} for the triangle sample whose PL image was depicted in Figure 3(b). It can be seen that the Raman image looks much more uniform with respect to the PL image. In particular, the central region of the triangle sample shows a relatively much weaker PL intensity compared with its edge regions, which is a common property found in most triangle samples, but not yet understood at moment. Meanwhile, the PL peak position of the triangle sample varies from 1.938 eV to 1.948 eV for different positions. Interestingly, it is found that the average PL peak position of the furnace-grown triangle sample is considerably smaller than that of the exfoliated monolayer at around 1.973 eV, as shown in Figure 3(d). This considerable difference in dominant PL peak position between the monolayer samples prepared in top-down and bottom-up methods should reflect to some extent the large difference in crystal quality of the two kinds of samples. It is well known that defects in crystals may introduce optically active band-tail states located at lower energy. As a result, PL emission band of crystal may redshift with increasing defect concentration. On the other hand, many defects may also introduce efficient non-radiative channels. Therefore, it is highly possible that the region with high defect concentration exhibits the emission band with a lower spectral center in energy and simultaneously a reduction in the overall intensity. The PL spectra in Figure 3(d) measured under the identical conditions show that the emission band of the furnace-grown triangle sample has an overall lower peak energy and intensity. In other words, the furnace-grown

triangle samples may have higher defect concentration. The relatively weak PL emission in the central region of the triangle samples is an indicator of higher concentration of defects in this region. In the CVD growth, the WS_2 monolayer formation was revealed to be due to expanding and thinning of the thick WS_{2+X} flakes through continuous heating.[11] This transformation process of monolayer starts from the center to side, so that the center region may have higher density of defects due to its longer exposure to high temperature, which causes the weaker PL intensity comparing to the side region.

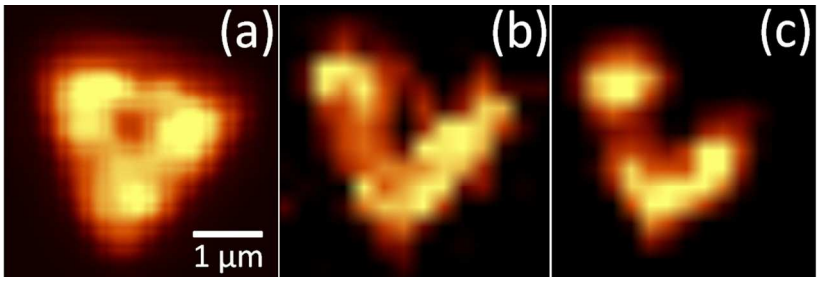

Figure 4. Three consecutive PL mappings on a triangle monolayer with laser power of 2 mW for each mapping time duration of 15 min.

At last, we want to address that long-time illuminating by focused laser beam may cause significant drop of the PL intensity of monolayer samples. Figure 4 shows three consecutive PL mapping images of a triangle WS_2 monolayer under the excitation of 2mW 514.5 nm focused laser beam for each mapping time duration of 15 min. The images show noticeable reducing in PL intensity after each PL mapping measurement. Therefore, it should be always very careful to optimize the laser power, the integration time and scanning resolution while performing optical mapping to 2D monolayer sheets.

Conclusions

To conclude, for Raman identification of monolayer WS_2, intensity change of the inter-layer phonon mode is more sensitive than shift amount of its peak position. Through mapping the two characteristic phonon modes, one can quickly distinguish the monolayer

region from the multilayers. On the other hand, PL mapping offers more details on the crystalline uniformity of the monolayer samples, and may give important information regarding defects. In response to the fast research development of 2D MX_2, PL and Raman mapping could offer a quick and reliable inspection on the size and uniformity of 2D MX_2, and thus of both scientific and technological significance.

Acknowledgements

One of the authors, S.J.X., would like to acknowledge support from the University Development Fund and the SRT on New Materials of HKU, as well as HK-UGC AoE Grants (Project No.: AoE/P-03/08). Dr. K.Q. Hong is gratefully acknowledged to grow the WS_2 triangle samples with bottom-up method. It is thankful that Dr. H.L. Zeng participated in the initial PL and Raman measurements of the exfoliated samples.

References

1 K. S. Novoselov, A. K. Geim, S. V. Morozov, D. Jiang, Y. Zhang, S. V. Dubonos, I. V. Grigorieva and A. A. Firsov, *Science,* 2004, **306,** 5696.
2 A. C. Ferrari, J. C. Meyer, V. Scardaci, C. Casiraghi, M. Lazzeri, F. Mauri, S. Piscanec, D. Jiang, K. S. Novoselov, S. Roth and A. K. Geim, *Phys. Rev. Lett.,* 2006, **97**, 187401.
3 A. C. Ferrari and D. M. Basko, *Nat. Nanotechnol*., 2013, **8**, 235.
4 D. J. Late, U. Maitra, L. S. Panchakarla, U. V. Waghmare and C. N. R. Rao, *J. Phys.: Condens. Matter*, 2011, **23**, 055303.
5 K. F. Mak, C. Lee, J. Hone, J. Shan and T. F. Heinz, *Phys. Rev. Lett.*, 2010, **105**, 136805.
6 H. S. S. R. Matte, A. Gomathi, A. K. Manna, D. J. Late, R. Datta, S. K. Pati and C. N. R. Rao, *Angew. Chem. Int. Ed.,* 2010, **122**, 4153.
7 H. R. Gutiérrez, N. Perea-López, A. L. Elías, A. Berkdemir, B. Wang, R. Lv, F. López-Urías, V. H. Crespi, H. Terrones and M. Terrones, *Nano Lett.,* 2013, **13**, 3447.
8 H. L. Zeng, G.-B. Liu, J. F. Dai, Y. J. Yan, B. R. Zhu, R. F. He, L. Xie, S. J. Xu, X. H. Chen, W. Yao and X. D. Cui, *Sci. Rep.,* 2013, **3**, 1608.
9 J.-G. Song, J. Park, W. Lee, T. Choi, H. Jung, C. W. Lee, S.-H. Hwang, J. M. Myoung, J.-H. Jung, S.-H. Kim, C. Lansalot-Matras and H. Kim, *ACS Nano,* 2013, **7** , 11333.
10 Y. Zhang, Y. Zhang, Q. Ji, J. Ju, H. Yuan, J. Shi, T. Gao, D. Ma, M. Liu, Y. Chen, X. Song, H. Y. Hwang, Y. Cui and Z. Liu, *ACS Nano,*2013, **7**, 8963.

11 C. Cong, J. Shang, X. Wu, B. Cao, N. Peimyoo, C. Qiu, L. Sun and T. Yu, *Adv. Opt. Mater.,* 2014, **2**, 131.
12 A. Ramasubramaniam, *Phys. Rev. B,* 2012, **86,** 115409.
13 A. Chernikov, T. C. Berkelbach, H. M. Hill, A. Rigosi, Y. Li, O. B. Aslan, D. R. Reichman, M. S. Hybertsen and T. F. Heinz, *Phys. Rev. Lett.,* 2014, **113,** 076802.
14 A. Molina-Sánchez and L. Wirtz, *Phys. Rev. B,* 2011, **84,** 155413.
15 C. Lee, H. Yan, L. E. Brus, T. F. Heinz, J. Hone and S. Ryu, *ACS Nano,* 2010, **4**, 2695.
16 A. Berkdemir, H. R. Gutierrez, A. R. Botello-Mendez, N. Perea-Lopez, A. L. Elias, C. I. Chia, B. Wang, V. H. Crespi, F. Lopez-Urias, J. C. Charlier, H. Terrones and M. Terrones, *Sci. Rep.,* 2013, **3**, 1755.
17 Y.-H. Lee, X.-Q. Zhang, W. Zhang, M.-T. Chang, C.-T. Lin, K.-D. Chang, Y.-C. Yu, J. T.-W. Wang, C.-S. Chang, L.-J. Li and T.-W. Lin, *Adv. Mater.,* 2012, **24**, 2320.
18 D. J. Late, Sharmila N. Shirodkar, U. V. Waghmare, V. P. Dravid and C. N. R. Rao, *ChemPhysChem*, 2014, **15**, 1592.
19 M. Thripuranthaka and D. J. Late, *ACS Appl. Mater. Interfaces*, 2014, **6**, 1158.
20 M. Thripuranthaka, R. V. Kashid, C. S. Rout and D. J. Late, *Appl. Phys. Lett*., 2014, **104**, 081911.
21 D. J. Late, T. Doneux and M. Bougouma, *Appl. Phys. Lett*., 2014, **105**, 233103.
22 S. R. Suryawanshi, P. S. Kolhe, C. S. Rout, D. J. Late and M. A. More, *Ultramicroscopy*, 2015, **149**, 51.
23 D. J. Late, B. Liu, H. S. S. Ramakrishna Matte, V. P. Dravid, and C. N. R. Rao, *ACS Nano*, 2012, **6**, 5635.
24 D. J. Late, et al., *ACS Appl. Mater. Interfaces*, 2014, **6**, 15881.